Front. Environ. Sci. Eng. 2022, 16(11): 137
https://doi.org/10.1007/s11783-022-1573-0

REVIEW ARTICLE

# Recent advances in special morphologic photocatalysts for $NO_x$ removal

**Yang Yang[1,2], Xiuzhen Zheng[2,3], Wei Ren[2], Jiafang Liu[2], Xianliang Fu (✉)[2], Sugang Meng[2], Shifu Chen[2], Chun Cai (✉)[1]**

1 School of Chemistry and Chemical Engineering, Nanjing University of Science and Technology, Nanjing 210094, China
2 Key Laboratory of Green and Precise Synthetic Chemistry and Applications, College of Chemistry and Material Science, Huaibei Normal University, Huaibei 235000, China
3 Shanghai Key Laboratory of Atmospheric Particle Pollution and Prevention (LAP[3]), Fudan University, Shanghai 200433, China

## HIGHLIGHTS

- Systematic information of recent progress in photocatalytic $NO_x$ removal is provided.
- The photocatalysts with special morphologies are reviewed and discussed.
- The morphology and photocatalytic $NO_x$ removal performance is related.

## GRAPHIC ABSTRACT

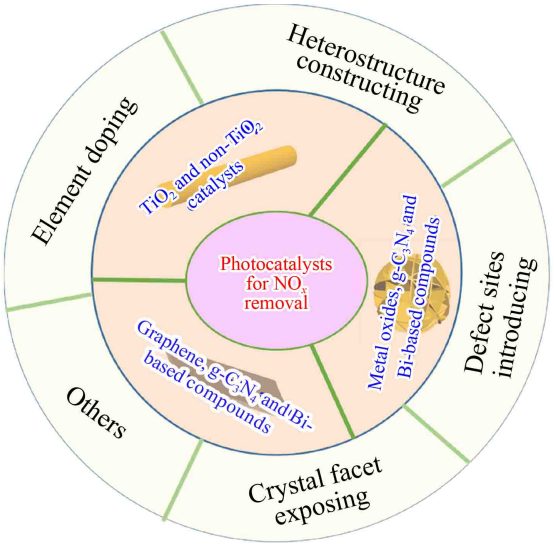


## ARTICLE INFO

*Article history:*
Received 10 January 2022
Revised 17 February 2022
Accepted 28 February 2022
Available online 28 April 2022

*Keywords:*
$NO_x$ removal
Photocatalyst
Graphene
$C_3N_4$
Bi-based compounds.

## ABSTRACT

The significant increase of $NO_x$ concentration causes severe damages to environment and human health. Light-driven photocatalytic technique affords an ideal solution for the removal of $NO_x$ at ambient conditions. To enhance the performance of $NO_x$ removal, 1D, 2D and 3D photocatalysts have been constructed as the light absorption and the separation of charge carriers can be manipulated through controlling the morphology of the photocatalyst. Related works mainly focused on the construction and modification of special morphologic photocatalyst, including element doping, heterostructure constructing, crystal facet exposing, defect sites introducing and so on. Moreover, the excellent performance of the photocatalytic $NO_x$ removal creates great awareness of the application, which has promising practical applications in $NO_x$ removal by paint (removing $NO_x$ indoor and outdoor) and pavement (degrading vehicle exhausts). For these considerations, recent advances in special morphologic photocatalysts for $NO_x$ removal was summarized and commented in this review. The purpose is to provide insights into understanding the relationship between morphology and photocatalytic performance, meanwhile, to promote the application of photocatalytic technology in $NO_x$ degradation.



## 1 Introduction

In recent years, air pollution has become an

✉ Corresponding authors
E-mails: fuxiliang@gmail.com (X. Fu); c.cai@njust.edu.cn (C. Cai)

environmental issue of general concern all over the world. With the social development, a series of environmental problems are brought due to the burning of fossil fuels, such as the emission of nitrogen oxides ($NO_x$), $SO_2$, CO and dust. In environmental science, $NO_x$ often refer to NO and $NO_2$ that cause air pollution, for instance, acid rain, ozone hole and photochemical smog (Hao et al., 2002). Furthermore, it can also have serious impacts on human health, irritating the eyes, nose, throat and lungs, easily destroying the human respiratory system, and causing diseases like bronchitis. In recent years, $NO_x$ caused by human activities have still continued to increase, leading to serious environmental problems and ecological hazards. As many countries have issued the relevant laws and regulations to limit the $NO_x$ emission, how to efficiently control the $NO_x$ emission has also become a hot issue in the environmental field.

At present, the commonly used methods to control the industrial $NO_x$ emission, include lye absorption, solid adsorption and selective oxidation reduction. However, these technologies have high operating costs for processing low-concentration $NO_x$ (~$10^{-3}$ mg/L). As an efficient technology to remove low-concentration air pollution, photocatalysis shows promising application prospect in $NO_x$ removal. Under the action of catalyst and sunlight, $NO_x$ can be oxidized to $NO_3^-$ or reduced to $N_2$. Generally, there are two kinds of degradation routs in the photocatalytic $NO_x$ removal, and one is using active species to oxidize $NO_x$, such as $h^+$, $\bullet O_2^-$, $H_2O_2$ and •OH. These radical groups can ultimately oxidize $NO_x$ to $NO_2$, $NO_2^-$ or $NO_3^-$, remaining on the surface of the photocatalyst. The other one is using $e^-$ to reduce $NO_x$, which can be decomposed into harmless $N_2$.

Since the researches on photocatalytic $NO_x$ removal have been carried out for nearly 40 years (Pichat et al., 1982), many semiconductors as catalysts have been developed and enormous efforts on photocatalysts have been made to improve the photocatalytic performance. Compared with nanoparticles and bulk materials, the photocatalysts with special morphology are paid more attention as the reactions often occur on the surface of the catalyst. Their size, dimensions, exposed crystal faces, and surface structure have direct impacts on the photocatalytic performance. Thus, controlling the photocatalyst morphology and studying the relationship between morphology and photocatalytic activity have become a hot research direction in the field of photocatalysis. To promote the application of photocatalytic technology in $NO_x$ degradation, the photocatalysts with special morphologies (from dimensions) are reviewed and discussed in this work, which may provide important reference for the related researchers.

## 2 1D nanostructural materials

Compared with nanoparticles and bulk materials, 1D nanomaterials, including nanowires, nanofibers, nanoribbons, nanorods and nanotubes, have a large specific surface area, unique electronic, optical and chemical properties. As photocatalysts, 1D structure constrains the lateral movement of $e^-$, guides $e^-$ to migrate along the axis, and provides a long enough migration channel for charge separation. These advantages make 1D materials as a good choose to improve the photocatalytic activity of $NO_x$ removal.

### 2.1 $TiO_2$-based materials

Many semiconductors can be used as photocatalysts, such as $TiO_2$, ZnO, $Fe_2O_3$ and $Bi_2O_3$, etc. Among them, $TiO_2$ has attracted enormous attention due to its stable property, non-toxicity and high photocatalytic-efficiency. Many researchers improve the photocatalytic activity of $NO_x$ removal by controlling $TiO_2$ morphology to form 1D nanostructures, like nanorods (Fig. 1(a)) (Habran et al., 2018), nanotubes (Figs.1(b) and 1(c)) (Li et al., 2015; Martin et al., 2017) and nanowires (Lee et al., 2020). Moreover, $TiO_2$ nanoparticles are deposited and coated on the supporter with 1D nanostructures, i.e., C nanotubes (Fig. 1(d)) (Xiao et al., 2019), C fiber (Kusiak-Nejman et al., 2020) and polymeric nanofibers (polyamide 6, polystyrene and polyurethane) (Szatmary et al., 2014). To improve the efficiency, some of these materials can also be used in photoelectrocatalytic $NO_x$ removal (Xiao et al., 2019; Dai et al., 2020).

However, $TiO_2$ as a wide-bandgap semiconductor, can only absorb the UV light. To increase its utilization of solar energy, element doping and semiconductor composite are important methods for 1D $TiO_2$ materials to obtain high photocatalytic activity in $NO_x$ removal. One or two element doping is commonly observed, like N-doped carbon quantum dots decorated on the surface of coral-like $TiO_{2-\delta}$ microstructures (Fig. 1(e)) (Ou et al., 2021), which could extend light absorption to longer wavelengths. To strengthen the effect of element doping, three elements are added to improve the $NO_x$ removal, for instance, $TiO_2$ nanotubes doped with Cu, Ce and B (Li et al., 2015). Compared with a single semiconductor, semiconductor composite is another important method to obtain better photocatalytic activity. $TiO_2$ can compound with many materials, such as $SnO_2$ (Huy et al., 2019), $WO_3$ (Liu et al., 2021) and $C_3N_4$ (Hossain et al., 2020). As the valence band, conduction band and band gap energies of two semiconductors are inconsistent, their band position will overlap. This behavior can not only facilitate the transfer and separation of photogenerated $e^-$ and $h^+$, but also expand the spectral response range of $TiO_2$.

### 2.2 Non-$TiO_2$ metal oxides and metal sulfides

ZnO, another widely used photocatalytic nanomaterial,

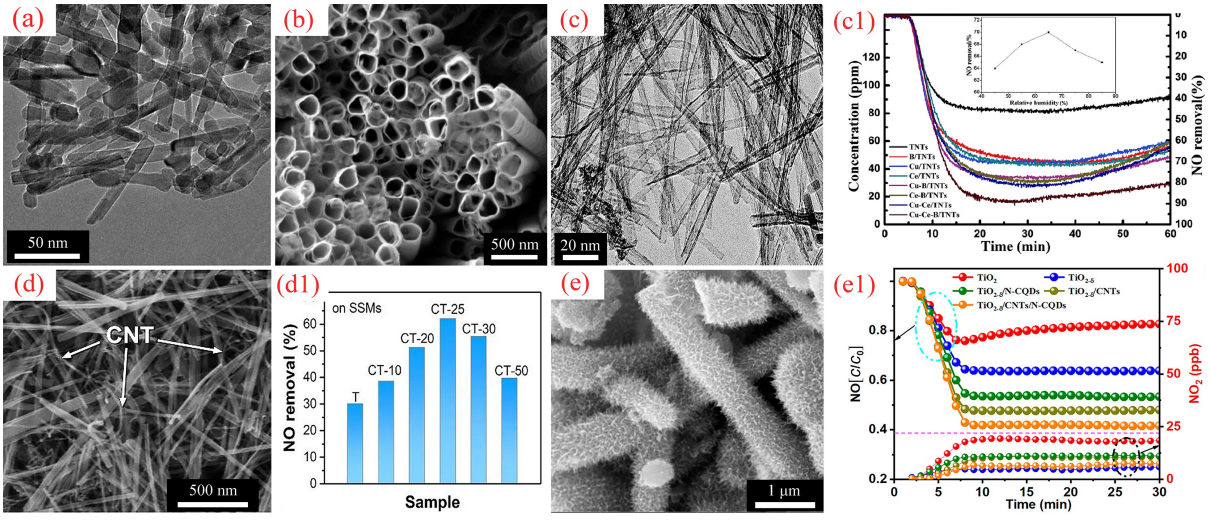


**Fig. 1** 1D $TiO_2$ material on photocatalytic NO degradation: nanorod (a, (Habran et al., 2018)), nanotube (b, (Martin et al., 2017), c, (Li et al., 2015)), nanoparticles on C nanotubes (d, (Xiao et al., 2019)) and coral (e, (Ou et al., 2021)). The figures are copyrighted from Taylor & Francis Publishing Group (a), Elsevier Publishing Group (b), Royal Society of Chemistry Publishing Group (c) and American Chemical Society Publishing Group (d, e).

has been studied to remove $NO_x$. To enhance the photocatalytic activity, some other semiconductors are compounding with its nanorod material, like g-$C_3N_4$/$Zn_2SnO_4N$ (Fig. 2(a), (Wang et al., 2019a)). Besides, other binary metal oxides with 1D nanostructure are investigated, such as $C_3N_4$/$Bi_2O_3$ (Fig. 2(b), (Hoang et al., 2020)) and $BiVO_4$/$Bi_2O_3$ (Fig. 2(c), (Huang et al., 2021)). For the ternary metal oxides, $ZnWO_4$ is widely investigated in the $NO_x$ removing, like Pd/$ZnWO_4$ (Fig. 2(d), (Chang et al., 2019)). Other multi-component metal oxides with 1D nanostructure are also studied, for instance, Au/BiOCl/BiOI (Wang et al., 2021c) and Ag/$Ag_2O$/SrSn$(OH)_6$ (Yang et al., 2021a). Moreover, some substrates with 1D fiber have been utilized to load active components, such as $Bi_2O_2CO_3$/$MoS_2$ on carbon nanofibers (Fig. 2(e), (Hu et al., 2017)). Recently, metal sulfides are also applied in the NO removal, such as Bi/CdS (Li et al., 2021) and Ag/$Bi_2S_3$ (Pham et al., 2021a).

## 3 2D nanostructural materials

Recently, 2D layered nanomaterials, as an important category of materials, have attracted intensive attention. They possess a series of excellent properties, such as good electrical and thermal conductivity, high electron mobility and excellent mechanical properties. According to the shape and thickness, they can be divided into nanosheets, nanoplates, nanowalls, nanoflakes and so on. Besides layered double hydroxides (Nehdi et al., 2022) and MXene (Wang et al., 2021d), the 2D nanomaterials commonly applied in photocatalytic $NO_x$ removal are mainly including graphene, g-$C_3N_4$ and Bi-based compounds.

### 3.1 Graphene and graphene oxide

Graphene is a single carbon atom layer, performing a 2D honeycomb lattice structure closely packed by a ring structure. Due to its special structure, graphene shows excellent electrical transport, mechanical and surface chemical properties. Especially, its 2D film-like structure and oxygen-containing functional groups on the surface (e.g., graphene oxide and reduced graphene oxide: GO and rGO) are conducive to embedding or loading other functional materials. Besides the elements doping (N and Bi (Feng et al., 2020)) on graphene (Fig. 3(a)), GO and rGO can bond with other materials to enhance the photocatalytic performance. For instance, GO can coupled with $C_3N_4$/$InVO_4$ cubes (Fig. 3(b), (Hu et al., 2018)), and $ZnCo_2O_4$ with rhombic dodecahedron are loaded on rGO (Fig. 3(c), (Xiao et al., 2018)).

### 3.2 $C_3N_4$

In recent decades, many scholars have shown an intense interest in photocatalytic technology and have made several important breakthroughs. In 2009, Wang et al. synthesized g-$C_3N_4$ by thermal polymerization (Wang et al., 2009). As a metal-free semiconductor photocatalyst, it shows promising prospects in photocatalytic field. However, from the perspective of application, the photocatalytic activity of pure $C_3N_4$ is not too high in $NO_x$ removal under visible light irradiation. To meet this challenge, many researchers have carried out a series of research work to regulate the internal electronic structure and increase the number of active sites, such as element dopant (Xia et al., 2022), heterojunction construction (Xie et al., 2022) and defect design (carbon vacancies (Gu

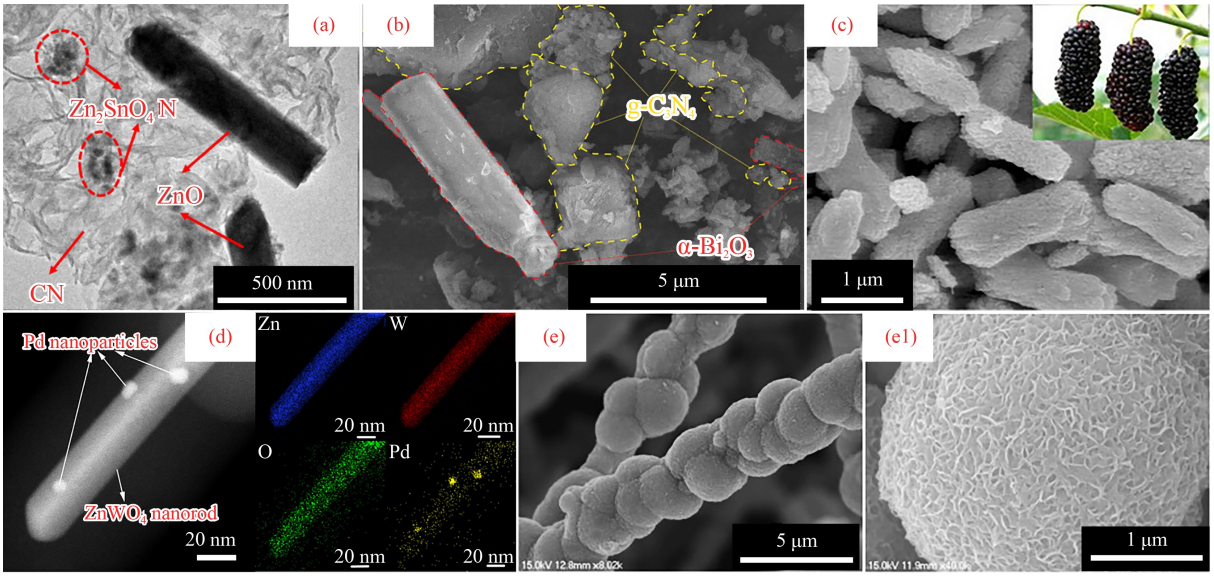


**Fig. 2** 1D non-$TiO_2$ metal oxide materials on photocatalytic NO degradation: ZnO nanorod (a, (Wang et al., 2019a)), $Bi_2O_3$ microrods (b, (Hoang et al., 2020)), mulberry-like $Bi_2O_3$ (c, (Huang et al., 2021)), $ZnWO_4$ nanorod (d, (Chang et al., 2019)) and $Bi_2O_2CO_3$/$MoS_2$ on carbon nanofibers (e, (Hu et al., 2017)). The figures are copyrighted from Elsevier Publishing Group (a, b and e), Wiley Publishing Group (c) and American Chemical Society Publishing Group (d).

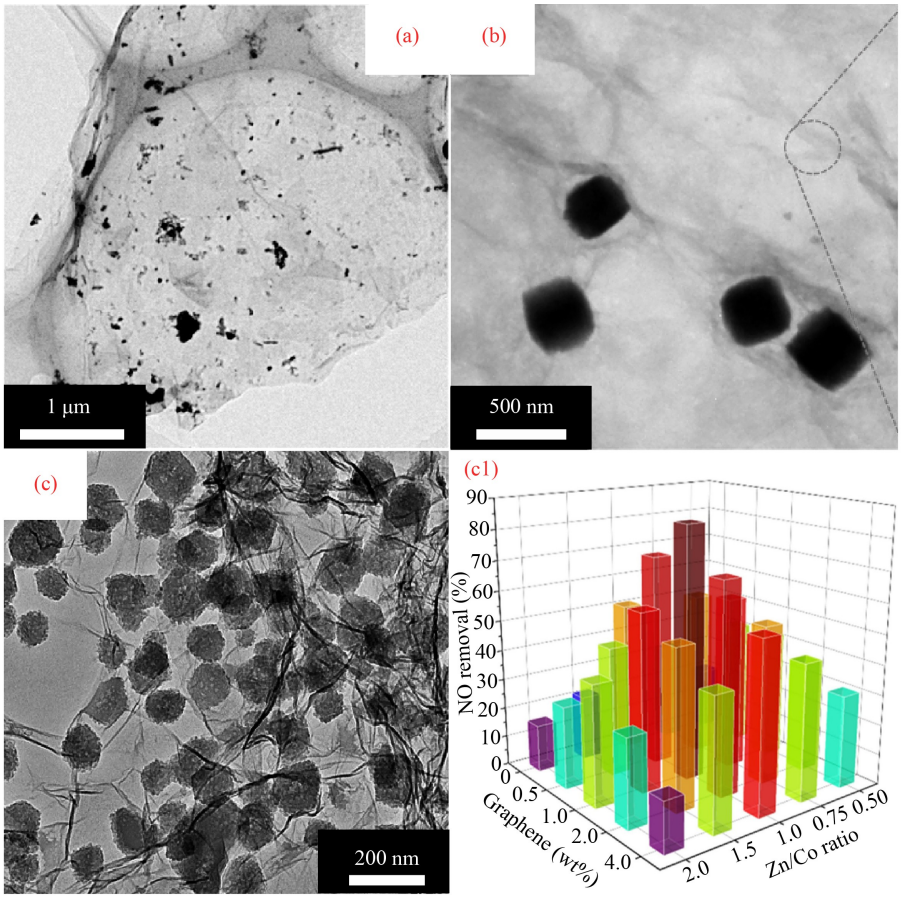


**Fig. 3** 2D GO-based materials loaded with different shapes on photocatalytic NO degradation: nanoparticles (a, (Feng et al., 2020)), cubes (b, (Hu et al., 2018)) and rhombic dodecahedron (c, (Xiao et al., 2018)). The figures are copyrighted from Royal Society of Chemistry Publishing Group (a) and Elsevier Publishing Group (b, c).

et al., 2020) and nitrogen vacancies (Duan et al., 2021)).

As $C_3N_4$ performs layer or sheet structure (Fig. 4(a)) (Han et al., 2019), the elements and semiconductors embedded on $C_3N_4$ are mainly nanoparticles, like Fig. 4(b) (Li et al., 2020a). Besides, some materials with special structure can also loaded on $C_3N_4$ surface, such as plate (Figs. 4(c) and 4(d)) (Wang et al., 2016; Geng et al., 2021b), cube (Fig. 4(e)) (Wang et al., 2021a), octahedra (Fig. 4(f)) (Ren et al., 2021) and sphere (Figs. 4(g) and 4(h)) (Dong et al., 2015; Wang et al., 2021b). Taking dual defects mediated $W_{18}O_{49}$/g-$C_3N_{4-x}$ heterojunction as an example (Fig. 4(h)), the Z-scheme heterojunction was achieved due to the formation of build-in electric field from g-$C_3N_{4-x}$ to $W_{18}O_{49}$ (Wang et al., 2021b). Combined with the promoted excision dissociation induced by N vacancies, the enhanced light absorption and accelerated carriers' separation induced by near-field enhancement effect in visible-NIR range of oxygen vacancies ($O_V$s). The NO removal rate of the composite could reach 83.55%, which was 1.41 and 6.15 times higher than that of $C_3N_4$ (59.14%) and $W_{18}O_{49}$ (13.59%).

### 3.3 Bi-based compounds

The development of new materials is the key to obtain the pioneering progress in many fields, and photocatalysis is no exception. Besides carbonaceous materials (Nikokavoura and Trapalis, 2018), many researchers explore and discover Bi-based photocatalysts, such as BiOX (X = Cl, Br and I), $Bi_2O_2CO_3$, $BiMO_x$ (M = W, Mo and Ge) and other 2D materials that absorb sunlight better. Due to its exposed surface, vacancy design and surface modification are easily performed, which is promising in material innovation and solving environmental problems (Zhao et al., 2021).

(1) BiOX (X = Cl, Br, I)

Bismuth oxyhalides (BiOX) are the semiconductor materials composed of three elements of Bi, O, and halogen atoms, in which X atoms are sandwiched by $Bi_2O_2$ atoms, and alternated to form the [X-Bi-O-Bi-X] structure. The built-in electric field formed by the negatively charged X layer and positively charged $[Bi_2O_2]^{2+}$ layer, which can effectively separate $h^+$ and $e^-$. This unique layered structure exhibits high stability and suitable band gap, consequently widely used in the field of photocatalysis, especially in environmental and energy fields.

BiOX are mainly including BiOCl (Figs. 5(a) and 5(b)) (Li et al., 2019a; Xie et al., 2020), BiOBr (Geng et al., 2021a; Hermawan et al., 2021) and BiOI (Zheng et al., 2021), which are performed sheet or plate structure. Additionally, other BiOX ($Bi_4O_5Br_2$ (Zhang et al., 2017), $Bi_{12}O_{17}Cl_2$, $Bi_3O_4Br$ and $Bi_{24}O_{31}Br_{10}$) are also applied in photocatalytic NO oxidation. In the work of Zhu et al., the subnanometer Ag/AgCl clusters were incorporated on atomically thin defective $Bi_{12}O_{17}Cl_2$ nanosheets via rebinding with unsaturated Cl atoms, resulting in an enhancement of photocatalytic activity for NO removal (Zhu et al., 2021). Moreover, the 2D BiOCl/$Bi_{12}O_{17}Cl_2$ composite were deeply studied by Zhang et al. (Zhang et al., 2018a), and it can couple with $MoS_2$ (Zhang et al.,

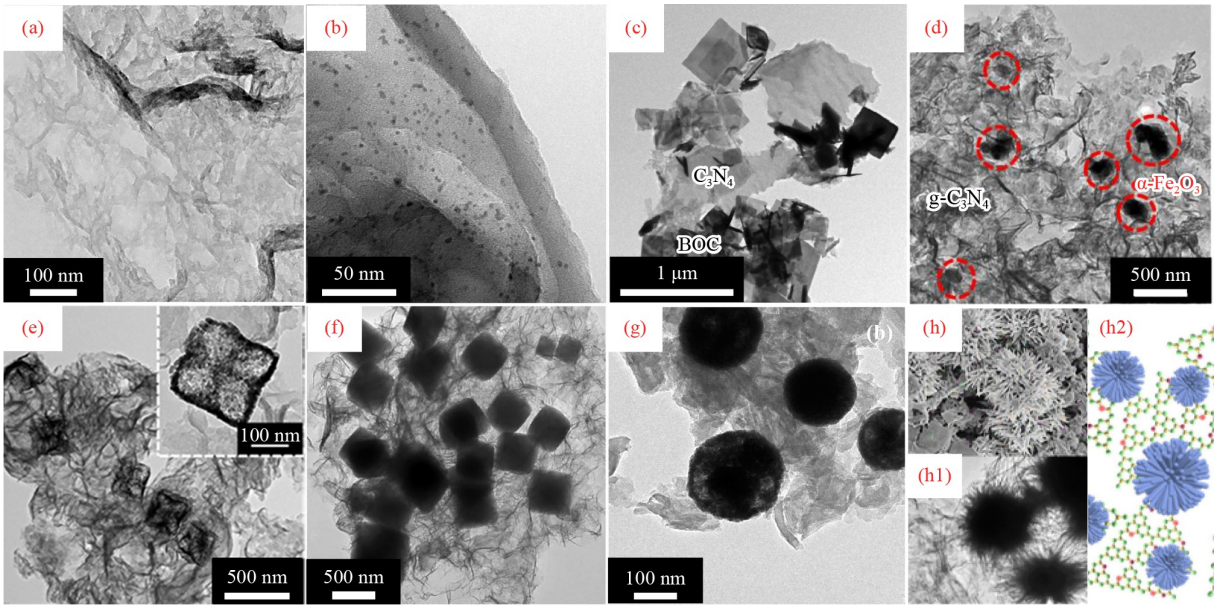


**Fig. 4** 2D $C_3N_4$ (a, (Han et al., 2019)) and its loaded materials with different shapes on photocatalytic NO degradation: nanoparticles (b, (Li et al., 2020a)), plates (c, (Wang et al., 2016)), hexagonal nanoplates (d, (Geng et al., 2021b)), hollow cubes (e, (Wang et al., 2021a)), octahedra (f, (Ren et al., 2021)), nanospheres (g, (Dong et al., 2015)) and spheres (h, (Wang et al., 2021b)). The figures are copyrighted from Elsevier Publishing Group (a, b, c, d, e, f and h) and American Chemical Society Publishing Group (g).

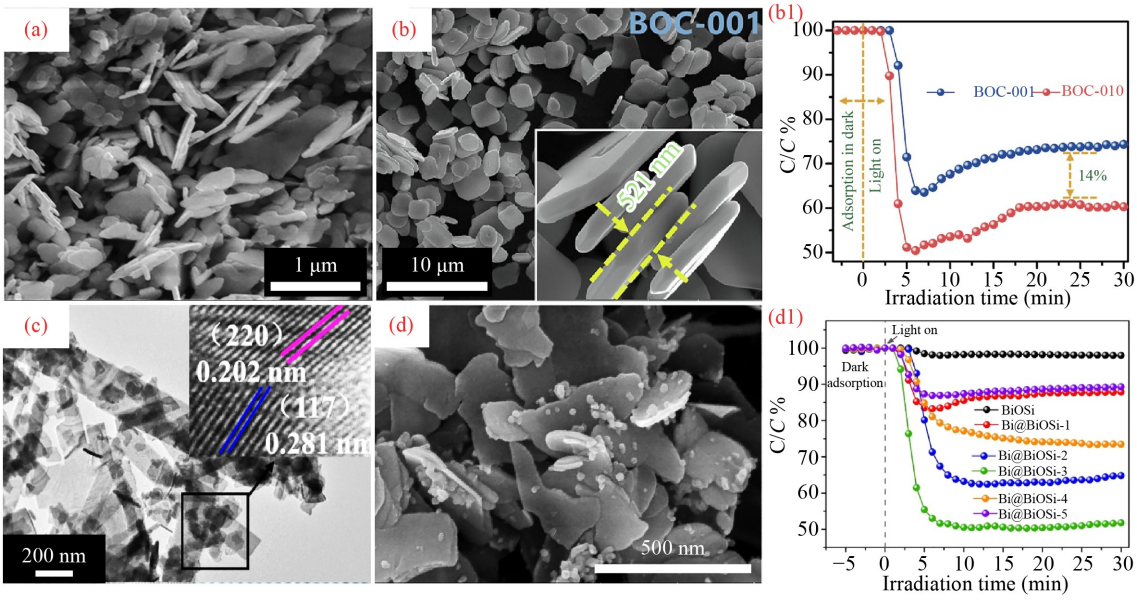


**Fig. 5** 2D Bi-based materials with plate shapes on photocatalytic NO degradation: BiOCl (a, (Xie et al., 2020), b, (Li et al., 2019a)), $Bi_{24}O_{31}Br_{10}/Bi_3O_4Br$ (c, (Li et al., 2020b) ) and $Bi/Bi_2O_2SiO_3$ (d, (Li et al., 2019d)). The figures are all copyrighted from Elsevier Publishing Group.

2019b), g-$C_3N_4$ (Zhang and Liang, 2019) and Ag/AgCl (Zhang et al., 2018b) to enhance the visible-light photocatalytic activity of NO removal. Furthermore, novel $Bi_{24}O_{31}Br_{10}/Bi_3O_4Br$ heterojunctions with a "nanosheet-on-ribbon" hierarchical structure was fabricated by Li et al. (Fig. 5(c), (Li et al., 2020b)). The special structure and interface interaction between $Bi_3O_4Br$ and $Bi_{24}O_{31}Br_{10}$ enhanced surface-active sites, prolonged light absorption, and promoted charge separation capability during the photocatalytic reaction.

(2) $Bi_2O_2CO_3$

$Bi_2O_2CO_3$ (BOC) is a sillen layered structure formed alternately by $[Bi_2O_2]^{2+}$ layer and $CO_3^{2-}$ layer. As the plane of the $CO_3^{2-}$ layer and $(Bi_2O_2)^{2+}$ layer is perpendicular to each other, its morphologies are performed nanosheets. In recent years, many researchers have studied BOC to remove NO by regulating defect sites (Lu et al., 2019b). Moreover, many materials are developed by compositing with it to improve the NO removal, such as graphene (Liu et al., 2020a), CdSe (Liu et al., 2019) and $ZnFe_2O_4$ (Huang et al., 2018).

(3) $BiMO_x$ (M = W, Mo and Ge)

Recently, $BiMO_x$ have been widely used in the field of photocatalysis due to their low toxicity, wide distribution of constituent elements, stable chemical properties, and easy adjustment of band structure. $BiMO_x$ have a unique anisotropic layered structure, and are easy to form a two-dimensional nanosheet structure with a high exposed surface during crystal growth. $Bi_2WO_6$ as an important bismuth oxide, is widely studied to remove $NO_x$, for example, $Cl/BiWO_4$ (Yang et al., 2021b) and black $P/Bi_2WO_6$ (Hu et al., 2019). Other bismuth oxides are also prepared to remove the NO pollutant, such as $Bi_2MoO_6$ (Ding et al., 2016; Wang et al., 2020) and $Bi/Bi_2GeO_5$ (Li et al., 2019c).

(4) Other bismuth materials

A model $Bi@Bi_2O_2SiO_3$ catalyst is described by Li et al., and this work has significant implications for modification of the abundant Bi-containing semiconductors (Fig. 5(d), (Li et al., 2019d)). The co-existed $O_V$ and Bi metal were demonstrated to have synergy effect on the reactant activation and catalyst surface. Moreover, I-doped BiOCOOH nanosheets was prepared via the replacement of $COOH^-$ ions with $I^-$ ions (Feng et al., 2018), which exhibited highly enhanced photocatalytic removal of NO in air by increasing visible light absorption and promoting charge separation.

## 4 3D nanostructural materials

3D structures are composed of low-dimensional materials (i.e., nanoparticles, nanoplates, nanowires, nanorods and nanosheets) as structural units to form spherical, flower, and dendritic structures. Due to the large surface energy of low-dimensional materials, the composition of hierarchical structure can effectively prevent the agglomeration of these low-dimensional materials, thereby facilitating the progress of the photocatalytic reaction. As 2D layers structure easily agglomerate to 3D structures, the $C_3N_4$ and Bi-based compounds as the research focuses are discussed in this section.

### 4.1 Metal oxides

There are many metal oxides with unique shape are constructed to remove $NO_x$. Spherical shape as a widely research focus is investigated by many scientific research workers, such as $Bi_2O_3$ (Figs. 6(a) and 6(d)) (Hojamberdiev et al., 2018; Rao et al., 2020), ZnO (Fig. 6(b)) (Chen et al., 2018), $TiO_2$ (Fig. 6(c)) (Sofianou et al., 2012) and other semiconductors. Besides spherical shape, some other special morphologies are also studied, for example, cubes (Pham et al., 2021b), rose (Fig. 6(e)) (Kowsari and Bazri, 2014), nanorod bundles (Fig. 6(f)) (Zhang et al., 2014), twin-brush (Fig. 6(g)) (Wu et al., 2021), decahedra (Xiao et al., 2016) and hexagonal (Fig. 6(h), (Kowsari and Abdpour, 2017) ) structure.

### 4.2 $C_3N_4$

As an important metal-free semiconductor, $C_3N_4$ with flower (Fig. 6(e), (Duan et al., 2019)) and sphere (Wang et al., 2022) can be fabricated by reunions of nanosheets. Besides Bi metal modified $C_3N_4$ to form a pomegranate-like structure (Li et al., 2017), a novel ball-in-ball structured g-$C_3N_4$@$SiO_2$ composite was constructed by Lin et al. (2017), which performs an excellent photocatalytic activity of NO removal as nano-photoreactor. Moreover, 3D foams consisted of g-$C_3N_4$ and $TiO_2$ quantum dots were prepared (Xiong et al., 2021), which provided abundant adsorption and activation sites for oxidizing NO flow gas under light irradiation.

### 4.3 Bi-based compounds

BiOX with the layer structure, can easily form flower and sphere shape assembled by nanoplates, such as BiOCl (Shen et al., 2021), BiOBr (Montoya-Zamora et al., 2020), BiOI (Fig. 7(a)) (Rao et al., 2019), $Bi_4O_5Br_2$ (Chang et al., 2021), $Bi_{12}O_{17}Br_2$ (Li et al., 2019b) and $Bi_5O_7I$ (Zhang et al., 2019a). For BOC, many elements can be added into its flowers to improve the selectivity and efficiency of photocatalytic NO oxidation (Fig. 7(b)) (Yuan et al., 2020). Moreover, it can couple with many semiconductor to form flower-like microspheres, for instance, $(BiO)_2CO_3$/$BiO_{2-x}$/graphene (Jia et al., 2019). Its NO removal efficiency was reached to 61%, and no obvious deactivation of the photocatalyst was caused by the photocatalytic process. Z-scheme charge transfer was

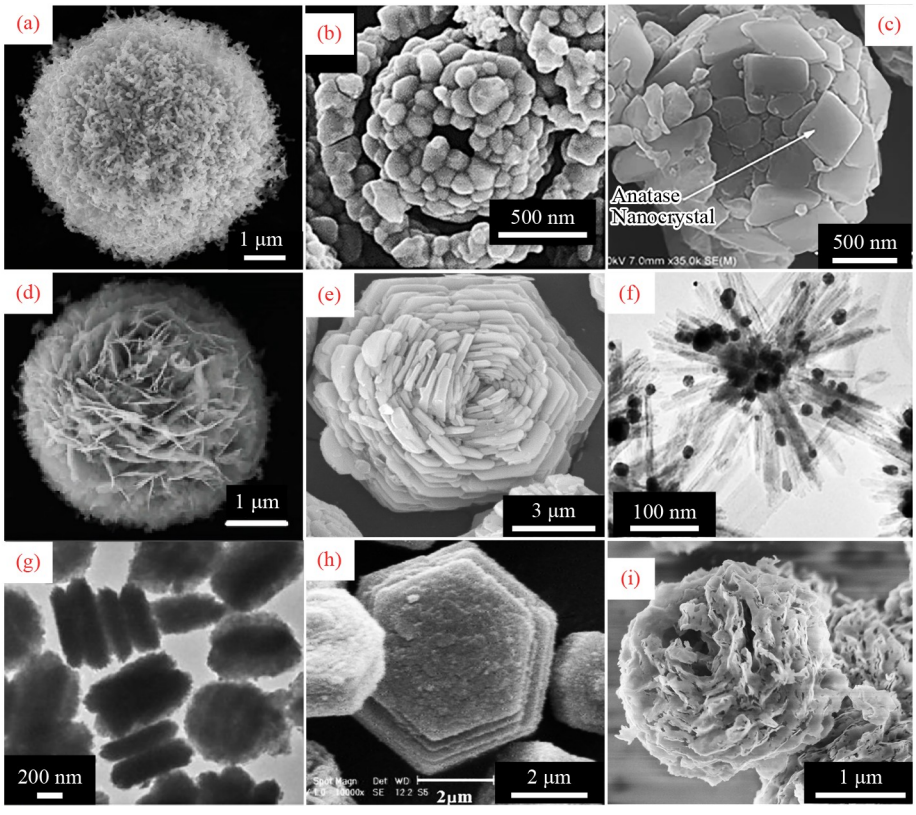


**Fig. 6** 3D metal oxides with different shapes on photocatalytic NO degradation, such as microspheres (a, (Hojamberdiev et al., 2018), b, (Chen et al., 2018), c, (Sofianou et al., 2012) and d, (Rao et al., 2020)), flower (e, (Kowsari and Bazri, 2014)), nanorod bundle (f, (Zhang et al., 2014)), twin-brush (g, (Wu et al., 2021)) and hexagon (h, (Kowsari and Abdpour, 2017)), and $C_3N_4$ materials with flower structure (i, (Duan et al., 2019)). The figures are copyrighted from Springer Publishing Group (a, c) Elsevier Publishing Group (b, e, f, g, h and i) and Wiley Publishing Group (d).

proposed to explain the observed high photocatalytic efficiency. The introduction of graphene is important because its high conductivity can promote the migration of $e^-$ and its 2D morphology can provide large surface area.

$Bi_2WO_6$ and $BiVO_4$ as the important ternary bismuth oxygen compound, are widely studied to remove $NO_x$. For $Bi_2WO_6$, some 3D hierarchical structured morphology composed of nanoplates are constructed, such as mesoporous flowers (Fig. 7(c)) (Lu et al., 2019a), rose-like (Wang et al., 2019b), microspheres (Fig. 7(d)) (Li et al., 2010) and octahedral cubic morphology (Liu et al., 2020b). Moreover, there are many beautiful shape of $BiVO_4$ are controllably synthesized by adjusting reaction condition, for example, hollow double-layer nanospheres (Fig. 7(e)) (Zha et al., 2021), microboats (Fig. 7(f)) (Ai and Lee, 2013) and eight-pot flower-like $BiVO_4$ (Fig. 7(g)) (Ou et al., 2015). To obtain high separation of photoinduced electron-hole pairs, Ou et al. designed a hierarchical g-$C_3N_4$@Ag/$BiVO_4$ hybrid photocatalyst, in which Ag was photodeposited on the preferred exposure (040) facets of $BiVO_4$ and subsequently g-$C_3N_4$ was covered on the surface of Ag/$BiVO_4$ (Fig. 7(h), (Ou et al., 2018)). Besides, other $BiMO_x$ samples with multi-level structure were also synthesized, like $Bi_2MoO_6$ microspheres (Huo et al., 2019), $Bi_2Sn_2O_{7-x}$ hollow nanocubes (Lu et al., 2021) and Bi/$BiPO_4$ nanosphere (Chen et al., 2020).

## 5 Conclusions

$NO_x$ from the burning of fossil fuels not only directly cause a series of environmental problems, but also bring harm to human life and health. Photocatalysis is currently considered as one of the most environmentally friendly technology in low-concentration $NO_x$ removal. In this review, we have investigated and classified the photocatalysts with special morphology for $NO_x$ removal, which are summarized in Tables 1, 2 and 3. This morphology research is beneficial for us to study the relationship between morphology and photocatalytic activity, and important for the development of "green environmental processes". Although many advanced materials with unique structure and high photocatalytic performance under visible light region have been reported, there is still a long way from academic research to practical application.

Nowadays, the photocatalyst practically applied in $NO_x$ removal are paint and pavement, which guide the direction of our researches. Photocatalytic paint is used in mechanically ventilated buildings to oxidize NO. Moreover, $TiO_2$ and $C_3N_4$ are applied in road construction to remove $NO_x$ from automobile exhaust gas. These preliminary study establishes the potential for heterogeneous photochemistry to occur on real application and opens the way for further research under realistic conditions. It is believed that photocatalytic $NO_x$ removal will be enriched to begin a revolution of renewable energy for practical benefits and future commercialization.

**Acknowledgements** This work was supported by the National Natural Science Foundation of China (Nos. 21607027, 52002142, 51772118, and 51972134), the Opening Project of Shanghai Key Laboratory of Atmospheric Particle Pollution and Prevention (LAP$^3$, No. FDLAP19007),

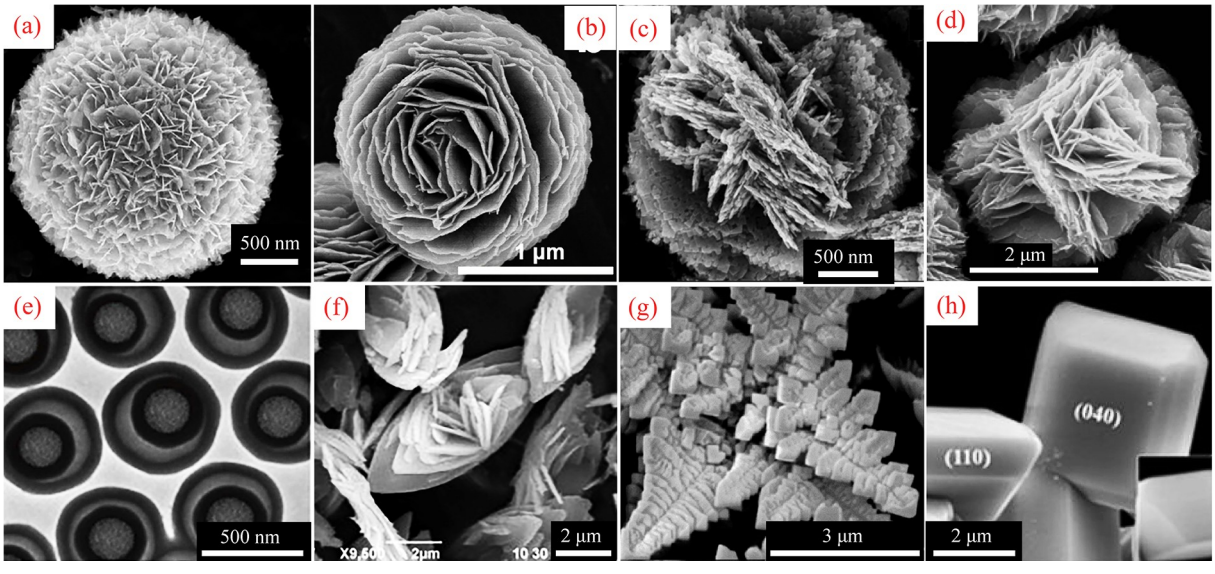


**Fig. 7** 3D Bi-based materials with different morphologies on photocatalytic NO degradation: flower (a, (Rao et al., 2019b), b, (Yuan et al., 2020)), hierarchical structure (c, (Lu et al., 2019a), d, (Li et al., 2010)), sphere (e, (Zha et al., 2021)), boat (f, (Ai and Lee, 2013)), eight-pot shape (g, (Ou et al., 2015)) and decagon shape (h, (Ou et al., 2018)). The figures are copyrighted from American Chemical Society Publishing Group (a, d), Elsevier Publishing Group (b, e, f and h), Springer Publishing Group (c) and Royal Society of Chemistry Publishing Group (g).

**Table 1** Summary of 1D photocatalysts for the $NO_x$ removal

| Photocatalysts | Light source | Pollutants (initial concentration, $\times10^{-3}$ mg/L) | Products | Removal efficiency | Ref. |
|---|---|---|---|---|---|
| $TiO_2$ nanorods | UV | NO (134) | – | 100% | Habran et al., 2018 |
| $TiO_2$ nanotubes | UV | $NO_x$ (1.34) | $NO_3^-$ | 60% | Martin et al., 2017 |
| Cu, Ce and B/$TiO_2$ nanotubes | UV | NO (201) | $HNO_3$ | 80% | Li et al., 2015 |
| Mn-graphene/$TiO_2$ nanowires | Fluorescent lamp | $NO_x$ (1.34) | $NO_2$, $NO_3^-$ | 25.4% | Lee et al., 2020 |
| $TiO_2$/C nanotubes | UV | NO (0.74 ) | $NO_3^-$ | 31.5% | Xiao et al., 2019 |
| Ag/$TiO_2$ on C fibers | UV | NO (2.68) | $NO_2$, nitric forms | 95% | Kusiak-Nejman et al., 2020 |
| $TiO_2$/polymeric nanofibers | UV | NO (1.34) | $NO_2$, $HNO_3$ | 16.2% | Szatmary et al., 2014 |
| $TiO_2$ nanorods | UV | NO (0.67) | $NO_3^-$ | 58% | Dai et al., 2020 |
| $TiO_{2-\delta}$/CNTs/N-CQDs corals | Visible light | NO (0.58) | $NO_3^-$ | 60.2% | Ou et al., 2021 |
| $SnO_2$/$TiO_2$ nanotubes | Visible light | NO (0.60) | $NO_3^-$ | 59.49% | Huy et al., 2019 |
| $WO_3$/$TiO_2$ nanorods/PDMS | Visible light | NO (26.8) | – | 61.41% | Liu et al., 2021 |
| g-$C_3N_4$/$TiO_2$ nanotubes | Visible light | NO (1.34) | $NO_2$, $NO_3^-$ | 19.62% | Hossain et al., 2020 |
| g-$C_3N_4$/$Zn_2SnO_4N$/ZnO nanorods | Visible light | NO (0.80) | – | 45.51% | Wang et al., 2019a |
| $C_3N_4$/$Bi_2O_3$ microrods | Visible light | NO (134) | $NO_2$, $NO_3^-$ | 39.1% | Hoang et al., 2020 |
| Mulberry-like $BiVO_4$/$Bi_2O_3$ | Visible light | NO (0.80) | – | 58.7% | Huang et al., 2021 |
| Pd/$ZnWO_4$ nanorods | Simulated sunlight | NO (0.58) | $NO_2^-$/$NO_3^-$ | 52.69% | Chang et al., 2019 |
| Au/BiOCl/BiOI rods | visible light | NO (0.74) | $NO_3^-$/$NO_2^-$ | 65.4% | Wang et al., 2021a |
| Ag/$Ag_2O$/$SrSn(OH)_6$ nanowires | Visible light | NO (0.74) | $NO_3^-$ | 45.1% | Yang et al., 2021a |
| $Bi_2O_2CO_3$/$MoS_2$ on carbon nanofibers | Visible light | NO (0.8) | $NO_3^-$ | 68% | Hu et al., 2017 |
| Bi/CdS nanorods | Visible light | NO (1.34 ) | $HNO_3$ | 58% | Li et al., 2021 |
| Ag/$Bi_2S_3$ nanorods | Solar light | NO (0.67) | $NO_3^-$ | 31.12% | Pham et al., 2021a |

**Table 2** Summary of 2D photocatalysts for the $NO_x$ removal

| Photocatalyst | Light source | Pollutants (initial concentration, $\times10^{-3}$ mg/L ) | Products | Removal efficiency | Ref. |
|---|---|---|---|---|---|
| MgAl–$CO_3$ layered double hydroxides | UV–Vis light | NO (0.67) | $NO_3^-$ | 60% | Nehdi et al., 2022 |
| $Nb_2O_5$/$Nb_2C$ MXene | Simulated sunlight | NO (0.67) | $HNO_3$ | 80% | Wang et al., 2021d |
| N, Bi/graphene nanosheets | UV | NO (0.67) | $NO_3^-$ | 49.5% | Feng et al., 2020 |
| g-$C_3N_4$/GO-$InVO_4$ layers | Visible light | NO (0.80) | $NO_3^-$ | 65% | Hu et al., 2018 |
| $ZnCo_2O_4$/rGO nanosheets | Visible light | NO (0.67) | $NO_3^-$ | 83.8% | Xiao et al., 2018 |
| B/$C_3N_4$ nanosheets | Visible light | NO (0.80) | $NO_3^-$ | 54% | Xia et al., 2022 |
| $FAPbBr_3$/g-$C_3N_4$ nanosheets | Visible light | NO (0.80) | $NO_3^-$ | 58% | Xie et al., 2022 |
| $C_3N_4$ lamellar structure | Visible light | NO (2.68) | $HNO_2$/$HNO_3$ | 33% | Gu et al., 2020 |
| $C_3N_4$ network structure | Visible light | NO (0.24) | $NO_3^-$ | 57.1% | Duan et al., 2021 |
| $C_3N_4$ nanosheets | Visible light | NO (20.1) | $NO_2$, $NO_2^-$, and $NO_3^-$ | 66.7% | Han et al., 2019 |
| Pd/g-$C_3N_4$ nanosheets | Visible light | NO (0.67) | $NO_3^-$ | 44.9% | Li et al., 2020a |
| $Bi_2O_2CO_3$/g-$C_3N_4$ layers | Visible light | NO (0.54) | $NO_3^-$ | 34.8% | Wang et al., 2016 |
| $Fe_2O_3$/g-$C_3N_4$ nanosheets | Visible light | NO (0.80) | $NO_3^-$ | 60.8% | Geng et al., 2021b |
| $NiCoO_x$/g-$C_3N_4$ nanosheets | Visible light | NO (0.80) | $NO_3^-$ | 59.1% | Wang et al., 2021a |
| $Sb_2WO_6$/g-$C_3N_4$ nanoflakes | Visible light | NO (0.80) | $NO_2^-$, $NO_3^-$ | 68% | Ren et al., 2021 |
| Bi/g-$C_3N_4$ nanosheets | Visible light | NO (0.80) | $HNO_2$, $HNO_3$ | 59.7% | Dong et al., 2015 |
| $W_{18}O_{49}$/g-$C_3N_{4-x}$ nanosheets | Simulated sunlight | NO (0.80) | – | 83.55% | Wang et al., 2021b |

(*Continued*)

| Photocatalyst | Light source | Pollutants (initial concentration, $\times10^{-3}$ mg/L ) | Products | Removal efficiency | Ref. |
|---|---|---|---|---|---|
| BiOCl nanosheets | Simulated sunlight | NO (0.54) | – | 23.7% | Xie et al., 2020 |
| BiOCl nanosheets | Uv360 | NO (0.67) | $NO_2^-$, $NO_3^-$ | 41% | Li et al., 2019a |
| Ba/BiOBr nanosheets | Visible light | NO (0.67) | $NO_3^-$ | 53% | Geng et al., 2021a |
| (Ti, C)-BiOBr/$Ti_3C_2T_x$ MXene layers | Simulated sunlight | NO (1.34) | $HNO_2$, $NO_3^-$ | 61% | Hermawan et al., 2021 |
| BiOI/BN nanosheets | Visible light | NO ($0.67x10^{-9}$) | $NO_2$ | 44.2% | Zheng et al., 2021 |
| $Bi_4O_5Br_2$ and $Bi_{12}O_{17}Br_2$ nanosheets | Visible light | NO (0.80) | $NO_3^-$ | 41.8% | Zhang et al., 2017 |
| Ag/AgCl/$Bi_{12}O_{17}Cl_2$ nanosheets | Visible light | NO | $NO_2$ | 25% | Zhu et al., 2021 |
| BiOCl/ $Bi_{12}O_{17}Cl_2$ nanoplates | Visible light | NO | $NO_3^-$ | 37.2% | Zhang et al., 2018a |
| $MoS_2$/BiOCl/$Bi_{12}O_{17}Cl_2$ nanosheets | Visible light | NO (0.67) | $NO_3^-$ | 51.1% | Zhang et al., 2019b |
| g-$C_3N_4$/BiOCl/$Bi_{12}O_{17}Cl_2$ nanosheets | Visible light | NO (0.67) | $NO_3^-$ | 46.8% | Zhang and Liang, 2019 |
| Ag/AgCl/BiOCl/$Bi_{12}O_{17}Cl_2$ nanosheets | Visible light | NO (0.67) | $NO_3^-$ | 49.5% | Zhang et al., 2018b |
| $Bi_3O_4Br$/$Bi_{24}O_{31}Br_{10}$ ribbon | Visible light | NO (0.54) | – | 32.5% | Li et al., 2020b |
| Bi/$Bi_2O_{2-x}CO_3$ nanosheets | Visible light | NO (67) | $NO_3^-$ | 50.5% | Lu et al., 2019b |
| graphene/N-$(BiO)_2CO_3$ nanosheets | Visible light | NO (0.74) | $NO_3^-$ | 53% | Liu et al., 2020a |
| CdSe/N-$(BiO)_2CO_3$ nanosheets | Visible light | NO (0.74) | $NO_3^-$ | 35% | Liu et al., 2019 |
| $ZnFe_2O_4$/$Bi_2O_2CO_3$ nanoplates | Visible light | NO (0.54) | $NO_3^-$ | 35% | Huang et al., 2018 |
| Cl/$BiWO_4$ nanosheets | Visible light | NO (0.80) | $NO_3^-$ | 64% | Yang et al., 2021b |
| Black P/$BiWO_4$ nanosheets | Visible light | NO (0.80) | $NO_3^-$ | 67% | Hu et al., 2019 |
| Bi/$Bi_2MoO_6$ nanoplates | Visible light | NO (0.80) | $NO_3^-$ | 41.4% | Ding et al., 2016 |
| Br/$Bi_2MoO_6$ microplates | Visible light | NO (0.83) | $NO_3^-$ | 62.9% | Wang et al., 2020 |
| Bi/$Bi_2GeO_5$ nanosheets | Visible light | NO (0.60) | $NO_2^-$, $NO_3^-$ | 56.2% | Li et al., 2019c |
| Bi@$Bi_2O_2SiO_3$ nanosheets | Visible light | NO (0.60) | $NO_2^-$, $NO_3^-$ | 50.2% | Li et al., 2019d |
| I/BiOCOOH nanoplates | Visible light | NO (0.74) | – | 49.7% | Feng et al., 2018 |

**Table 3** Summary of 3D photocatalysts for the $NO_x$ removal

| Photocatalyst | Light source | Pollutants (initial concentration, $\times10^{-3}$ mg/L) | Products | Removal efficiency | Ref. |
|---|---|---|---|---|---|
| $MoS_2$/$Bi_2O_3$ microspheres | Visible light | NO (0.58) | $NO_2$, $NO_2^-$ or $NO_3^-$ | 41.4% | Hojamberdiev et al., 2018 |
| Pd/PdO/$Bi_2O_3$ microspheres | Visible light | NO (0.58) | $NO_2^-$, $NO_3^-$ | 47.6% | Rao et al., 2020 |
| ZnO microspheres | UV365 | NO (0.54) | $NO_3^-$ | 77.3% | Chen et al., 2018 |
| $TiO_2$ nanospheres | UV | NO (1.34) | $NO_2$, $NO_3^-$ | 7% | Sofianou et al., 2012 |
| $ZnSn(OH)_6$ cubes | Solar light | NO (0.67) | $NO_2$, $NO_3^-$ | 74.5% | Pham et al., 2021b |
| Mg/ZnO rosette | UV | $SO_2$, $NO_x$, and CO (1.34) | $HNO_2$/$HNO_3$ | 23% | Kowsari and Bazri, 2014 |
| Au/$TiO_2$ nanorod bundles | Visible light | NO (0.54) | $NO_2$, $NO_3^-$ | 31% | Zhang et al., 2014 |
| Ag/ZnO twin-brush | Simulated sunlight | NO (0.67) | $NO_3^-$ | 71% | Wu et al., 2021 |
| CNT/$TiO_2$ decahedron | UV365 | NO (0.67) | $NO_2$, $NO_3^-$ | 76.8% | Xiao et al., 2016 |
| ZnO hexagon | UV | NO (2.68) | $HNO_2$/$HNO_3$ | 56% | Kowsari and Abdpour, 2017 |
| $C_3N_4$ flower | Visible light | NO (0.80) | – | 59.7% | Duan et al., 2019 |
| BiOCl/g-$C_3N_4$ spheres | Visible light | NO (0.80) | $NO_3^-$ | 56.1% | Wang et al., 2022 |
| Bi/$C_3N_4$ pomegranate | Visible light | NO (0.80) | – | 70.4% | Li et al., 2017 |
| g-$C_3N_4$@$SiO_2$ microsphere | Visible light | NO (0.80) | $NO_2^-$, $NO_3^-$ | 29.6% | Lin et al., 2017 |
| $C_3N_4$/$TiO_2$ foam | Visible light | NO (0.74) | $NO_2$, $NO_3^-$ | 65% | Xiong et al., 2021 |

(*Continued*)

| Photocatalyst | Light source | Pollutants (initial concentration, $\times10^{-3}$ mg/L) | Products | Removal efficiency | Ref. |
|---|---|---|---|---|---|
| $Mn_3O_4$/BiOCl microflowers | Simulated solar light | NO (0.13) | $HNO_2$, $NO_3^-$ | 75% | Shen et al., 2021 |
| BiOBr microspheres | UV-visible light | NO (1.34) | $NO_3^-$ | 95% | Montoya-Zamora et al., 2020 |
| Zn/BiOI microspheres | Visible light | NO (0.58) | $NO_3^-$ | 53.6% | Rao et al., 2019 |
| $Bi_4O_5Br_2$-GO clusters | Visible light | NO (0.74) | $NO_3^-$ | 53% | Chang et al., 2021 |
| BiOBr/$Bi_{12}O_{17}Br_2$ flowers | Simulated solar light | NO (0.54) | – | 57.3% | Li et al., 2019b |
| Au, La/$Bi_5O_7I$ microspheres | Visible light | NO (0.54) | $NO_2^-$, $NO_3^-$ | 54.5% | Zhang et al., 2019a |
| La/$Bi_2O_2CO_3$ microspheres | Visible light | NO (0.67) | $NO_2^-$/$NO_3^-$ | 49.8% | Yuan et al., 2020 |
| $(BiO)_2CO_3$/$BiO_{2-x}$/graphene microspheres | Simulated solar light | NO (0.58) | $NO_3^-$ | 61% | Jia et al., 2019 |
| I/$Bi_2WO_6$ microflowers | Simulated solar light | NO (0.58) | $NO_3^-$ | 50% | Lu et al., 2019a |
| $Bi_2WO_6$ rosette | Visible light | NO (670) | $NO_3^-$ | 54% | Wang et al., 2019b |
| $Bi_2WO_6$ microsphere | Visible light | NO (0.54) | $NO_3^-$ | 52% | Li et al., 2010 |
| $Bi_2WO_6$/$NH_2$-UiO-66 octahedral cubes | Visible light | NO (0.67) | $NO_3^-$/$NO_2^-$ | 79% | Liu et al., 2020b |
| $BiVO_4$/$Bi_2S_3$ spheres | Visible light | NO (402) | $NO_3^-$ | 37.7% | Zha et al., 2021 |
| $BiVO_4$ boats | Visible light | NO (0.54) | $HNO_2$, $HNO_3$ | 35.4% | Ai and Lee, 2013 |
| $BiVO_4$ flowers | Visible light | NO (536) | $NO_3^-$ | 48.5% | Ou et al., 2015 |
| g-$C_3N_4$@Ag/$BiVO_4$ decagon | Visible light | NO (536) | $NO_3^-$ | 83% | Ou et al., 2018 |
| $CO_3$-$Bi_2MoO_6$ micro/nanospheres | Visible light | NO (0.74) | $NO_3^-$ | 34% | Huo et al., 2019 |
| $Bi_2Sn_2O_{7-x}$ hollow nanocubes | Visible light | NO (0.54) | $NO_2^-$, $NO_3^-$ | 32% | Lu et al., 2021 |
| Bi/$BiPO_4$ nanospheres | Visible light | NO (0.54) | $NO_3^-$ | 32.8% | Chen et al., 2020 |

and some Foundation of Anhui Province in China: Natural Science Foundation (Nos. 1808085J24 and 2108085MB43), the University Natural Science Research Project (No. KJ2020A0126), and the Cultivating Outstanding Talents (No. gxbjZD2020066).

## References

Ai Z H, Lee S (2013). Morphology-dependent photocatalytic removal of NO by hierarchical $BiVO_4$ microboats and microspheres under visible light. Applied Surface Science, 280: 354–359

Chang F, Yang C, Wang J Y, Lei B, Li S J, Kim H (2021). Enhanced photocatalytic conversion of $NO_x$ with satisfactory selectivity of 3D-2D $Bi_4O_5Br_2$-GO hierarchical structures via a facile microwave-assisted preparation. Separation and Purification Technology, 266: 118237

Chang L, Zhu G, Hassan Q U, Cao B, Li S, Jia Y, Gao J, Zhang F, Wang Q (2019). Synergetic effects of $Pd^0$ metal nanoparticles and $Pd^{2+}$ ions on enhanced photocatalytic activity of $ZnWO_4$ nanorods for nitric oxide removal. Langmuir, 35(35): 11265–11274

Chen M J, Li X W, Huang Y, Yao J, Li Y, Lee S C, Ho W K, Huang T T, Chen K H (2020). Synthesis and characterization of Bi-$BiPO_4$ nanocomposites as plasmonic photocatalysts for oxidative NO removal. Applied Surface Science, 513: 145775

Chen X L, Zhang H Q, Zhang D Q, Miao Y C, Li G S (2018). Controllable synthesis of mesoporous multi-shelled ZnO microspheres as efficient photocatalysts for NO oxidation. Applied Surface Science, 435: 468–475

Dai W, Tao Y, Zou H, Xiao S, Li G, Zhang D, Li H (2020). Gas-phase photoelectrocatalytic oxidation of NO *via* $TiO_2$ nanorod array/FTO photoanodes. Environmental Science & Technology, 54(9): 5902–5912

Ding X, Ho W K, Shang J, Zhang L Z (2016). Self doping promoted photocatalytic removal of no under visible light with $Bi_2MoO_6$: Indispensable role of superoxide ions. Applied Catalysis B: Environmental, 182: 316–325

Dong F, Zhao Z, Sun Y, Zhang Y, Yan S, Wu Z (2015). An advanced semimetal-organic Bi spheres-g-$C_3N_4$ nanohybrid with SPR-enhanced visible-light photocatalytic performance for NO purification. Environmental Science & Technology, 49(20): 12432–12440

Duan Y, Wang Y, Gan L, Meng J, Feng Y, Wang K, Zhou K, Wang C, Han X, Zhou X (2021). Amorphous carbon nitride with three coordinate nitrogen ($N_3C$) vacancies for exceptional $NO_x$ abatement in visible light. Advanced Energy Materials, 11(19): 2004001

Duan Y Y, Li X F, Lv K L, Zhao L, Liu Y (2019). Flower-like g-$C_3N_4$ assembly from holy nanosheets with nitrogen vacancies for efficient NO abatement. Applied Surface Science, 492: 166–176

Feng X, Li X W, Cui W, Dong F, Zhang T R (2018). An ion-exchange strategy for I-doped BiOCOOH nanoplates with enhanced visible light photocatalytic $NO_x$ removal. Pure and Applied Chemistry, 90(2): 353–361

Feng Z J, Lian D R, Wu X, Liu Y, Jia W, Yuan X Y (2020). The synergy of N-doped and SPR-promoted photocatalytic removal of NO with graphene/Bi nanocomposites. RSC Advances, 10(5): 2734–2739

Geng Q, Xie H T, Cui W, Sheng J P, Tong X, Sun Y J, Li J Y, Wang Z M, Dong F (2021a). Optimizing the electronic structure of BiOBr Nanosheets via Combined Ba doping and oxygen vacancies for promoted photocatalysis. Journal of Physical Chemistry C, 125(16): 8597–8605

Geng Y, Chen D, Li N, Xu Q, Li H, He J, Lu J (2021b). Z-Scheme 2D/2D α-$Fe_2O_3$/g-$C_3N_4$ heterojunction for photocatalytic oxidation of nitric oxide. Applied Catalysis B: Environmental, 280: 119409

Gu Z Y, Cui Z T, Wang Z J, Qin K S, Asakura Y, Hasegawa T, Tsukuda S, Hongo K, Maezono R, Yin S (2020). Carbon vacancies and hydroxyls in graphitic carbon nitride: Promoted photocatalytic NO removal activity and mechanism. Applied Catalysis B: Environmental, 279: 119376

Habran M, Krambrock K, Maia da Costa M E H, Morgado E Jr, Marinkovic B A (2018). $TiO_2$ anatase nanorods with non-equilibrium crystallographic {001} facets and their coatings exhibiting high photo-oxidation of NO gas. Environmental Technology, 39(2): 231–239

Han D Y, Liu J, Cai H, Zhou X, Kong L R, Wang J W, Shi H F, Guo Q, Fan X X (2019). High-yield and low-cost method to synthesize large-area porous g-$C_3N_4$ nanosheets with improved photocatalytic activity for gaseous nitric oxide and 2-propanol photodegradation. Applied Surface Science, 464: 577–585

Hao J, Tian H, Lu Y (2002). Emission inventories of $NO_x$ from commercial energy consumption in China, 1995-1998. Environmental Science & Technology, 36(4): 552–560

Hermawan A, Hasegawa T, Asakura Y, Yin S (2021). Enhanced visible-light-induced photocatalytic $NO_x$ degradation over (Ti, C)-BiOBr/$Ti_3C_2T_x$ MXene nanocomposites: Role of Ti and C doping. Separation and Purification Technology, 270: 118815

Hoang T V T, Minh T C, Van V P (2020). Enhancing photocatalysis of NO gas degradation over g-$C_3N_4$ modified α-$Bi_2O_3$ microrods composites under visible light. Materials Letters, 281: 128637

Hojamberdiev M, Zhu G, Lu H, Kumar M, Wang M, Gao J (2018). $MoS_2$ quantum dots-modified porous β-$Bi_2O_3$ microspheres with enhanced visible-light-induced photocatalytic activity for Bisphenol A degradation and NO removal. Journal of Materials Science, 30(3): 2610–2621

Hossain S M, Park H, Kang H J, Mun J S, Tijing L, Rhee I, Kim J H, Jun Y S, Shon H K (2020). Modified hydrothermal route for synthesis of photoactive anatase $TiO_2$/g-CN nanotubes from sludge generated $TiO_2$. Catalysts, 10(11): 1350

Hu J, Chen D, Mo Z, Li N, Xu Q, Li H, He J, Xu H, Lu J (2019). Z-scheme 2D/2D heterojunction of black phosphorus/monolayer $Bi_2WO_6$ nanosheets with enhanced photocatalytic activities. Angewandte Chemie (International ed. in English), 58(7): 2073–2077

Hu J D, Chen D Y, Li N J, Xu Q F, Li H, He J H, Lu J M (2017). In situ fabrication of $Bi_2O_2CO_3$/$MoS_2$ on carbon nanofibers for efficient photocatalytic removal of NO under visible-light irradiation. Applied Catalysis B: Environmental, 217: 224–231

Hu J D, Chen D Y, Li N J, Xu Q F, Li H, He J H, Lu J M (2018). Fabrication of graphitic-$C_3N_4$ quantum dots/graphene-$InVO_4$ aerogel hybrids with enhanced photocatalytic NO removal under visible-light irradiation. Applied Catalysis B: Environmental, 236: 45–52

Huang L, Hou D F, Gan S L, Qiao X Q, Li D S (2021). Multifunctional mulberry-like $BiVO_4$-$Bi_2O_3$ p-n heterostructures with enhanced both photocatalytic reduction and oxidation activities. ChemCatChem, 13(14): 3357–3367

Huang Y, Zhu D D, Zhang Q, Zhang Y F, Cao J J, Shen Z X, Ho W K, Lee S C (2018). Synthesis of a $Bi_2O_2CO_3$/$ZnFe_2O_4$ heterojunction with enhanced photocatalytic activity for visible light irradiation-induced NO removal. Applied Catalysis B: Environmental, 234: 70–78

Huo W, Xu W, Cao T, Guo Z, Liu X, Ge G, Li N, Lan T, Yao H C, Zhang Y, Dong F (2019). Carbonate doped $Bi_2MoO_6$ hierarchical nanostructure with enhanced transformation of active radicals for efficient photocatalytic removal of NO. Journal of Colloid and Interface Science, 557: 816–824

Huy T H, Bui D P, Kang F, Wang Y F, Liu S H, Thi C M, You S J, Chang G M, Pham V V (2019). $SnO_2$/$TiO_2$ nanotube heterojunction: The first investigation of NO degradation by visible light-driven photocatalysis. Chemosphere, 215: 323–332

Jia Y, Li S, Gao J, Zhu G, Zhang F, Shi X, Huang Y, Liu C (2019). Highly efficient $(BiO)_2CO_3$-$BiO_{2-x}$-graphene photocatalysts: Z-Scheme photocatalytic mechanism for their enhanced photocatalytic removal of NO. Applied Catalysis B: Environmental, 240: 241–252

Kowsari E, Abdpour S (2017). In-situ functionalization of mesoporous hexagonal ZnO synthesized in task specific ionic liquid as a photocatalyst for elimination of $SO_2$, $NO_x$, and CO. Journal of Solid State Chemistry, 256: 141–150

Kowsari E, Bazri B (2014). Synthesis of rose-like ZnO hierarchical nanostructures in the presence of ionic liquid/$Mg^{2+}$ for air purification and their shape-dependent photodegradation of $SO_2$, $NO_x$, and CO. Applied Catalysis A-General, 475: 325–334

Kusiak-Nejman E, Czyżewski A, Wanag A, Dubicki M, Sadłowski M, Wróbel R J, Morawski A W (2020). Photocatalytic oxidation of nitric oxide over AgNPs/$TiO_2$-loaded carbon fiber cloths. Journal of Environmental Management, 262: 110343

Lee J C, Gopalan A I, Saianand G, Lee K P, Kim W J (2020). Manganese and graphene included titanium dioxide composite nanowires: Fabrication, characterization and enhanced photocatalytic activities. Nanomaterials (Basel, Switzerland), 10(3): 456

Li G, Zhang D, Yu J C, Leung M K (2010). An efficient bismuth tungstate visible-light-driven photocatalyst for breaking down nitric oxide. Environmental Science & Technology, 44(11): 4276–4281

Li J Y, Chen R M, Cen W L, Yan P, Li K L, Wang P, Shu S, Chu Y H, Dong F (2019a). Quantifying the activation energies of ROS-induced $NO_x$ conversion: Suppressed toxic intermediates generation and clarified reaction mechanism. Chemical Engineering Journal, 375: 122026

Li K, He Y, Chen P, Wang H, Sheng J, Cui W, Leng G, Chu Y, Wang Z, Dong F (2020a). Theoretical design and experimental investigation on highly selective Pd particles decorated $C_3N_4$ for safe photocatalytic NO purification. Journal of Hazardous Materials, 392: 122357

Li R, Feng J Q, Zhang X C, Xie F X, Liu J X, Zhang C M, Wang Y W, Yue X P, Fan C M (2020b). *In situ* reorganization of $Bi_3O_4Br$ nanosheet on the $Bi_{24}O_3Br_{10}$ ribbon structure for superior visible-light photocatalytic capability. Separation and Purification Technology, 247: 117007

Li R, Ou X, Zhang L, Qi Z, Wu X, Lu C, Fan J, Lv K (2021). Photocatalytic oxidation of NO on reduction type semiconductor photocatalysts: Effect of metallic Bi on CdS nanorods. Chemical Communications, 57(78): 10067–10070

Li R, Xie F, Liu J, Zhang C, Zhang X, Fan C (2019b). Room-temperature hydrolysis fabrication of $BiOBr/Bi_{12}O_{17}Br_2$ Z-Scheme photocatalyst with enhanced resorcinol degradation and NO removal activity. Chemosphere, 235: 767–775

Li R M, Dong G J, Chen G M (2015). Synthesis, characterization and performance of ternary doped Cu-Ce-B/$TiO_2$ nanotubes on the photocatalytic removal of nitrogen oxides. New Journal of Chemistry, 39(9): 6854–6863

Li X W, Zhang W D, Cui W, Li J Y, Sun Y J, Jiang G M, Huang H W, Zhang Y X, Dong F (2019c). Reactant activation and photocatalysis mechanisms on Bi-metal@$Bi_2GeO_5$ with oxygen vacancies: A combined experimental and theoretical investigation. Chemical Engineering Journal, 370: 1366–1375

Li X W, Zhang W D, Li J Y, Jiang G M, Zhou Y, Lee S, Dong F (2019d). Transformation pathway and toxic intermediates inhibition of photocatalytic NO removal on designed Bi metal@defective $Bi_2O_2SiO_3$. Applied Catalysis B: Environmental, 241: 187–195

Li Y H, Lv K L, Ho W K, Zhao Z W, Huang Y (2017). Enhanced visible-light photo-oxidation of nitric oxide using bismuth-coupled graphitic carbon nitride composite heterostructures. Chinese Journal of Catalysis, 38(2): 321–329

Lin B, Chen S, Dong F, Yang G (2017). A ball-in-ball g-$C_3N_4$@$SiO_2$ nano-photoreactor for highly efficient $H_2$ generation and NO removal. Nanoscale, 9(16): 5273–5279

Liu G Y, Xia H Y, Niu Y H, Zhao X, Zhang G T, Song L F, Chen H X (2021). Fabrication of self-cleaning photocatalytic durable building coating based on $WO_3$-TNs/PDMS and NO degradation performance. Chemical Engineering Journal, 409: 128187

Liu Y, Yu S, Zheng K W, Chen W W, Dong X A, Dong F, Zhou Y (2019). NO photo-oxidation and in-situ DRIFTS studies on N-doped $Bi_2O_2CO_3$/CdSe quantum dot composite. Journal of Inorganic Materials, 34(4): 425–432

Liu Y, Zhou Y, Yu S, Xie Z H, Chen Y, Zheng K W, Mossin S, Lin W H, Meng J, Pullerits T, Zheng K B (2020a). Defect state assisted Z-scheme charge recombination in $Bi_2O_2CO_3$/graphene quantum dot composites for photocatalytic oxidation of NO. ACS Applied Nano Materials, 3(1): 772–781

Liu Y Q, Zhou Y, Tang Q J, Li Q, Chen S, Sun Z X, Wang H Q (2020b). A direct Z-scheme $Bi_2WO_6$/$NH_2$-UiO-66 nanocomposite as an efficient visible-light-driven photocatalyst for NO removal. RSC Advances, 10(3): 1757–1768

Lu X, Zhu G Q, Zhang R X, Li S P, Pan L K, Nie J L, Rao F (2019a). I-doped $Bi_2WO_6$ microflowers enhanced visible light photocatalytic activity for organic pollution degradation and NO removal. Journal of Materials Science Materials in Electronics, 30(19): 17787–17797

Lu Y F, Chen M J, Huang T T, Huang Y, Cao J J, Li H W, Ho K, Lee S C (2021). Oxygen vacancy-dependent photocatalytic activity of well-defined $Bi_2Sn_2O_{7-x}$ hollow nanocubes for $NO_x$ removal. Environmental Science. Nano, 8(7): 1927–1933

Lu Y F, Huang Y, Zhang Y F, Huang T T, Li H W, Cao J J, Ho W K (2019b). Effects of $H_2O_2$ generation over visible light-responsive $Bi/Bi_2O_{2-x}CO_3$ nanosheets on their photocatalytic $NO_x$ removal performance. Chemical Engineering Journal, 363: 374–382

Montoya-Zamora J M, Martinez-De La Cruz A, Lopez-Cuellar E, Pérez González F A (2020). BiOBr photocatalyst with high activity for $NO_x$ elimination. Advanced Powder Technology, 31(8): 3618–3627

Martin M, Leonid S, Tomáš R, Jan Š, Jaroslav K, Mariana K, Michaela J, František P, Gustav P (2017). Anatase $TiO_2$ nanotube arrays and titania films on titanium mesh for photocatalytic $NO_x$ removal and water cleaning. Catalysis Today, 287: 59–64

Nehdi A, Frini-Srasra N, de Miguel G, Pavlovic I, Sánchez L, Fragoso J (2022). Use of LDH- chromate adsorption co-product as an air purification photocatalyst. Chemosphere, 286(Pt 2): 131812

Nikokavoura A, Trapalis C (2018). Graphene and g-$C_3N_4$ based photocatalysts for $NO_x$ removal: A review. Applied Surface Science, 430: 18–52

Ou M, Nie H, Zhong Q, Zhang S, Zhong L (2015). Controllable synthesis of 3D $BiVO_4$ superstructures with visible-light-induced photocatalytic oxidation of NO in the gas phase and mechanistic analysis. Physical chemistry chemical physics: PCCP, 17(43): 28809–28817

Ou M, Wan S P, Zhong Q, Zhang S L, Song Y, Guo L N, Cai W, Xu Y L (2018). Hierarchical Z-scheme photocatalyst of g-$C_3N_4$@Ag/$BiVO_4$ (040) with enhanced visible-light-induced photocatalytic oxidation performance. Applied Catalysis B: Environmental, 221: 97–107

Ou Y, Zhu G, Rao F, Gao J, Chang J, Xie X, Zhang W, Huang Y, Hojamberdiev M (2021). Coral-shaped $TiO_{2-\delta}$ decorated with carbon quantum dots and carbon nanotubes for NO removal. ACS Applied Nano Materials, 4(7): 7330–7342

Pham M T, Hussain A, Bui D P, Nguyen T M T, You S J, Wang Y F (2021a). Surface plasmon resonance enhanced photocatalysis of Ag nanoparticles-decorated $Bi_2S_3$ nanorods for NO degradation. Environmental Technology & Innovation, 23: 101755

Pham M T, Tran H H, Nguyen T M T, Bui D P, Huang Y, Cao J, You S J, Van Viet P, Nam V H, Wang Y F (2021b). Revealing De$NO_x$ and DeVOC reactions via the study of the surface and bandstructure of $ZnSn(OH)_6$ photocatalysts. Acta Materialia, 215: 117068

Pichat P, Herrmann J M, Courbon H, Disdier J, Mozzanega M N (1982). Photocatalytic oxidation of various compounds over $TiO_2$ and other semiconductor oxides; Mechanistic considerations. Canadian Journal of Chemical Engineering, 60(1): 27–32

Rao F, Zhu G, Wang M, Zubairu S M, Peng J, Gao J, Hojamberdiev M (2020). Constructing the Pd/PdO/β-$Bi_2O_3$ microspheres with enhanced photocatalytic activity for Bisphenol A degradation and NO removal. Journal of Chemical Technology and Biotechnology (Oxford, Oxfordshire), 95(3): 862−874

Rao F, Zhu G Q, Hojamberdiev M, Zhang W B, Li S P, Gao J Z, Zhang F C, Huang Y H, Huang Y (2019). Uniform $Zn^{2+}$-doped BiOI microspheres assembled by ultrathin nanosheets with tunable oxygen vacancies for super-stable removal of NO. Journal of Physical Chemistry C, 123(26): 16268–16280

Ren Y Y, Li Y, Wu X Y, Wang J L, Zhang G K (2021). S-scheme $Sb_2WO_6$/g-$C_3N_4$ photocatalysts with enhanced visible-light-induced photocatalytic NO oxidation performance. Chinese Journal of Catalysis, 42(1): 69–77

Shen T, Shi X K, Guo J X, Li J, Yuan S D (2021). Photocatalytic removal of NO by light-driven $Mn_3O_4$/BiOCl heterojunction

photocatalyst: Optimization and mechanism. Chemical Engineering Journal, 408: 128014

Sofianou M V, Trapalis C, Psycharis V, Boukos N, Vaimakis T, Yu J, Wang W (2012). Study of $TiO_2$ anatase nano and microstructures with dominant {001} facets for NO oxidation. Environmental Science and Pollution Research International, 19(9): 3719–3726

Szatmáry L, Šubrt J, Kalousek V, Mosinger J, Lang K (2014). Low-temperature deposition of anatase on nanofiber materials for photocatalytic $NO_x$ removal. Catalysis Today, 230: 74–78

Wang B B, Chen D Y, Li N J, Xu Q F, Li H, He J H, Lu J M (2021a). Enhanced photocatalytic oxidation of nitric oxide to MOF-derived hollow bimetallic oxide microcubes supported on g-$C_3N_4$ nanosheets via p-n heterojunction. Industrial & Engineering Chemistry Research, 60(7): 2921–2930

Wang M, Tan G, Dang M, Wang Y, Zhang B, Ren H, Lv L, Xia A (2021b). Dual defects and build-in electric field mediated direct Z-scheme $W_{18}O_{49}$/g-$C_3N_{4-x}$ heterojunction for photocatalytic NO removal and organic pollutant degradation. Journal of Colloid and Interface Science, 582(Pt A): 212−226

Wang M, Tan G Q, Ren H J, Xia A, Liu Y (2019a). Direct double Z-scheme O-g-$C_3N_4$/$Zn_2SnO_4$N/ZnO ternary heterojunction photocatalyst with enhanced visible photocatalytic activity. Applied Surface Science, 492: 690–702

Wang M, Wang B, Xie B, Li N, Xu Q, Li H, He J, Chen D, Lu J (2022). Ultrathin Two-Dimensional BiOCl with oxygen vacancies anchored in three-dimensional porous g-$C_3N_4$ to construct a hierarchical Z-scheme heterojunction for the photocatalytic degradation of NO. Industrial & Engineering Chemistry Research, 61(1): 317–329

Wang S Y, Ding X, Yang N, Zhan G M, Zhang X H, Dong G H, Zhang L Z, Chen H (2020). Insight into the effect of bromine on facet-dependent surface oxygen vacancies construction and stabilization of $Bi_2MoO_6$ for efficient photocatalytic NO removal. Applied Catalysis B: Environmental, 265: 118585

Wang X, Maeda K, Thomas A, Takanabe K, Xin G, Carlsson J M, Domen K, Antonietti M (2009). A metal-free polymeric photocatalyst for hydrogen production from water under visible light. Nature Materials, 8(1): 76–80

Wang X, Zhu J, Fu X, Xu J, Yu X, Zhu Y, Zhang Y, Zhu M (2021c). Boosted visible-light photocatalytic performance of Au/BiOCl/BiOI by high-speed spatial electron transfer channel. Journal of Alloys and Compounds, 890: 161736

Wang Y, Hu X, Song H, Cai Y, Li Z, Zu D, Zhang P, Chong D, Gao N, Shen Y, Li C (2021d). Oxygen vacancies in actiniae-like $Nb_2O_5$/$Nb_2C$ MXene heterojunction boosting visible light photocatalytic NO removal. Applied Catalysis B: Environmental, 299: 120677

Wang Y N, Zeng Y Q, Zhang S L, Zhong Q (2019b). Synthesis of 3D hierarchical rose-like $Bi_2WO_6$ superstructure with enhanced visible-light-induced photocatalytic performance. JOM, 71(6): 2112–2119

Wang Z Y, Huang Y, Ho W K, Cao J J, Shen Z X, Lee S C (2016). Fabrication of $Bi_2O_2CO_3$/g-$C_3N_4$ heterojunctions for efficiently photocatalytic NO in air removal: In-situ self-sacrificial synthesis, characterizations and mechanistic study. Applied Catalysis B: Environmental, 199: 123–133

Wu F, Pu C, Zhang M, Liu B, Yang J (2021). Silver embedded in defective twin brush-like ZnO for efficient and stable photocatalytic NO removal. Surfaces and Interfaces, 25: 101298

Xia X, Xie C, Xu B, Ji X, Gao G, Yang P (2022). Role of B-doping in g-$C_3N_4$ nanosheets for enhanced photocatalytic NO removal and $H_2$ generation. Journal of Industrial and Engineering Chemistry, 105: 303–312

Xiao S, Wan Z, Zhou J, Li H, Zhang H, Su C, Chen W, Li G, Zhang D, Li H (2019). Gas-phase photoelectrocatalysis for breaking down nitric oxide. Environmental Science & Technology, 53(12): 7145–7154

Xiao S, Zhu W, Liu P, Liu F, Dai W, Zhang D, Chen W, Li H (2016). CNTs threaded (001) exposed $TiO_2$ with high activity in photocatalytic NO oxidation. Nanoscale, 8(5): 2899–2907

Xiao S N, Pan D L, Liang R, Dai W R, Zhang Q T, Zhang G Q, Su C L, Li H X, Chen W (2018). Bimetal MOF derived mesocrystal $ZnCo_2O_4$ on rGO with High performance in visible-light photocatalytic NO oxidization. Applied Catalysis B: Environmental, 236: 304–313

Xie B, Chen D, Li N, Xu Q, Li H, He J, Lu J (2022). Fabrication of an $FAPbBr_3$/g-$C_3N_4$ heterojunction to enhance NO removal efficiency under visible-light irradiation. Chemical Engineering Journal, 430: 132968

Xie F X, Li R, Zhang X C, Wang Y W, Fan C M (2020). In situ growth of BiOCl thin film on Bi plate for photocatalytic application. Materials Letters, 260: 126937

Xiong M W, Tao Y, Zhao Z S, Zhu Q, Jin X Q, Zhang S Q, Chen M, Li G S (2021). Porous g-$C_3N_4$/$TiO_2$ foam photocatalytic filter for treating NO indoor gas. Environmental Science. Nano, 8(6): 1571–1579

Yang L, Yu Y, Yang W, Li X, Zhang G, Shen Y, Dong F, Sun Y (2021a). Efficient visible light photocatalytic NO abatement over $SrSn(OH)_6$ nanowires loaded with Ag/$Ag_2O$ cocatalyst. Environmental Research, 201: 111521

Yang X L, Wang S Y, Chen T, Yang N, Jiang K, Wang P, Li S, Ding X, Chen H (2021b). Chloridion-induced dual tunable fabrication of oxygen-deficient $Bi_2WO_6$ atomic layers for deep oxidation of NO. Chinese Journal of Catalysis, 42(6): 1013–1023

Yuan C, Chen R, Wang J, Wu H, Sheng J, Dong F, Sun Y (2020). La-doping induced localized excess electrons on $(BiO)_2CO_3$ for efficient photocatalytic NO removal and toxic intermediates suppression. Journal of Hazardous Materials, 400: 123174

Zha R, Niu Y, Liu C, He L, Zhang M (2021). Oxygen vacancy configuration in confined $BiVO_4$-$Bi_2S_3$ heterostructures promotes photocatalytic oxidation of NO. Journal of Environmental Chemical Engineering, 9(6): 106586

Zhang D Q, Wen M C, Zhang S S, Liu P J, Zhu W, Li G S, Li H X (2014). Au nanoparticles enhanced rutile $TiO_2$ nanorod bundles with high visible-light photocatalytic performance for NO oxidation. Applied Catalysis B: Environmental, 147: 610–616

Zhang J, Zhu G, Li S, Rao F, Hassan Q U, Gao J, Huang Y, Hojamberdiev M (2019a). Novel Au/La-$Bi_5O_7I$ microspheres with efficient visible-light photocatalytic activity for NO removal: Synergistic effect of Au nanoparticles, La doping, and oxygen vacancy. ACS Applied Materials & Interfaces, 11(41): 37822–37832

Zhang W, Liang Y (2019). Facile synthesis of ternary g-$C_3N_4$@BiOCl/

$Bi_{12}O_{17}Cl_2$ composites with excellent visible light photocatalytic activity for NO removal. Frontiers in Chemistry, 7: 231

Zhang W D, Dong X A, Jia B, Zhong J B, Sun Y J, Dong F (2018a). 2D BiOCl/$Bi_{12}O_{17}Cl_2$ nanojunction: Enhanced visible light photocatalytic NO removal and in situ DRIFTS investigation. Applied Surface Science, 430: 571–577

Zhang W D, Dong X A, Liang Y, Liu R, Sun Y J, Dong F (2019b). Synergetic effect of BiOCl/$Bi_{12}O_{17}Cl_2$ and $MoS_2$: *in situ* DRIFTS investigation on photocatalytic NO oxidation pathway. Rare Metals, 38(5): 437–445

Zhang W D, Dong X G, Liang Y, Sun Y J, Dong F (2018b). Ag/AgCl nanoparticles assembled on BiOCl/$Bi_{12}O_{17}Cl_2$ nanosheets: Enhanced plasmonic visible light photocatalysis and in situ DRIFTS investigation. Applied Surface Science, 455: 236–243

Zhang W D, Liu X L, Dong X A, Dong F, Zhang Y X (2017). Facile synthesis of $Bi_{12}O_{17}Br_2$ and $Bi_4O_5Br_2$ nanosheets: *In situ* DRIFTS investigation of photocatalytic NO oxidation conversion pathway. Chinese Journal of Catalysis, 38(12): 2030–2038

Zhao C, Pan X, Wang Z H, Wang C C (2021). 1+1 > 2: A critical review of MOF/bismuth-based semiconductor composites for boosted photocatalysis. Chemical Engineering Journal, 417: 128022

Zheng Q, Cao Y H, Huang N J, Zhang R Y, Zhou Y (2021). Selective exposure of BiOI oxygen-rich {110} facet induced by BN nanosheets for enhanced photocatalytic oxidation performance. Chinese Journalof Chemical Physics, 37(8): 2009063

Zhu L, Wu Y, Wu S, Dong F, Xia J, Jiang B (2021). Tuning the active sites of atomically thin defective $Bi_{12}O_{17}Cl_2$ via incorporation of subnanometer clusters. ACS Applied Materials & Interfaces, 13(7): 9216–9223